Applied Physics A (2020) 126:434
https://doi.org/10.1007/s00339-020-03611-5

Applied Physics A
Materials Science & Processing

Antimicrobial behavior of leached Al–Cu–Fe-based quasicrystals

Aqib Zahoor[1] · Taha Aziz[1] · Soumble Zulfiqar[2] · Aisha Sadiq[3] · Rashid Ali[1] · Rub Nawaz Shahid[1] · Naeem ul Haq Tariq[1] · Attaullah Shah[4] · Khurram Shehzad[5] · Fahad Ali[1] · Hasan Bin Awais[1]

Received: 7 February 2020 / Accepted: 6 May 2020

Abstract
In this study, for the first time, antimicrobial properties of Al–Cu–Fe, Al–Cu–Fe–B and Al–Cu–Fe–Co quasicrystal powders were investigated in the leached and un-leached condition against Gram-negative (*E. aerogenes, K. pneumoniae)* and Gram-positive (*B. cereus, K. rosea)* bacterial environment. Leaching of the powders in 10 M NaOH aqueous solution resulted in the enrichment of Cu and Fe at the surface. Consequently, bacterial activities in the vicinity of the leached quasicrystal powders were inhibited, indicating good antimicrobial characteristics of the leached powders. All the three leached powder samples exhibited antimicrobial activities with a varying degree. From the diameter of inhibition zone, it was deduced that *E. aerogenes* are the most susceptible against the leached powders. The leached Al–Cu–Fe–B and Al–Cu–Fe–Co quasicrystal powders showed nanostructured features on the outer surface. During leaching, the icosahedral structure was retained in all the samples.

Keywords Quasicrystals · Gram-negative · Gram-positive · Thermal spray deposition · Mechanical milling · Hot pressing · Antimicrobial activities · Icosahedral

1 Introduction

Over the years, efforts have been made to develop new materials that could be used to fight against infections and provide sterilized surface [1]. The major growing concern of health-associated infections (HAIs) is to control and prevent the infections around the world [2]. Clinical evidence shows that copper and silver have intrinsic ability to reduce the microorganism's burden on the surface [1]. However, quasicrystalline (QC) materials have never been explored to assess their antimicrobial properties. QCs possess distinct structure which is neither crystalline nor amorphous [3]. QCs were first reported in 1984 [4], and this discovery led to Dan Shechtman getting the Noble Prize in Chemistry in 2011 [5]. QCs possess perfect long range order without translation periodicity and show the sharp diffraction pattern like crystalline materials, but they have forbidden symmetries (i.e., fivefold and tenfold) [6, 7]. Due to complex structure of QCs, they possess exclusive physical properties including low thermal and electrical conductivity [8, 9], high hardness [10], low coefficient of thermal expansion [11], low coefficient of friction [12] and good corrosion resistance [13]. Interest in QCs, as an antimicrobial agent, was developed due to the formation of Cu-enriched nano-regions on the leached surface of bulk QC [14]. The above-mentioned characteristics motivate us to study the antimicrobial properties of the QCs. In addition, QCs have much higher hardness value and wear resistance when compared with those of copper and silver. Therefore, leached quasicrystalline surface can more effectively be used for variety of components used in hospitals or at places where both wear resistance and antibacterial characteristics are required. In the USA, annually almost 1.7 million people got infected from the frequently touched surfaces, such as doorknobs, bed rails and water taps while visiting hospital [15].

✉ Fahad Ali
fahadali62@hotmail.com

1 Department of Metallurgy and Materials Engineering, Pakistan Institute of Engineering and Applied Sciences, Islamabad (PIEAS), Islamabad 45650, Pakistan

2 School of Biological Sciences, University of the Punjab, Lahore, Pakistan

3 Forman Christian College, Lahore, Pakistan

4 National Institute of Laser and Optronics, Islamabad, Pakistan

5 Physics Division, PINSTECH, Islamabad, Pakistan

Published online: 20 May 2020

In order to examine the antimicrobial properties of QCs materials, Al–Cu–Fe, Al–Cu–Fe–B and Al–Cu–Fe–Co QC powder samples were investigated in detail. The major constituents of these QCs are Al, Cu and Fe which are non-toxic, economical and easily available in the market [16, 17]. Moreover, Al-based QCs can be leached in alkaline solutions such as NaOH or Na_2CO_3 in order to make their surface active [18–20]. In the literature, various hypotheses have been proposed to explain antimicrobial activity of Cu. Among these hypotheses, the most commonly recognized mechanism is that the membrane of bacteria ruptures when they make contact with Cu surface. The resulting surface leakage leads to the loss of cell content and eventually leads to cell death [21].

The aim of this study is to explore the antimicrobial properties of QCs against Gram-negative (*E. aerogenes, K. pneumoniae)* and Gram-positive (*B. cereus, K. rosea)* bacteria. The QC powders, synthesized by thermal spray deposition and mechanical alloying methods, were tested for their antimicrobial activity in leached and un-leached condition by Kirby–Bauer (disk diffusion) test. The results showed remarkably high antimicrobial activity of the leached QCs. Our results showed that copper containing QCs could be a new and better material with excellent mechanical and prospective antimicrobial properties.

2 Materials and methods

2.1 Powder preparation

Three types of quasicrystalline (QC) alloy powders, with the nominal composition $Al_{62.5}Cu_{25}Fe_{12.5}$, $Al_{65}Cu_{23}Fe_{11}B$ and $Al_{65}Cu_{23}Fe_{11}Co$, were used in this study. The Al–Cu–Fe quasicrystals were obtained after thermal spray deposition [22]. The QCs of Al–Cu–Fe–B and Al–Cu–Fe–Co were prepared by mechanical alloying followed by hot pressing. High-purity elemental powders were mechanically

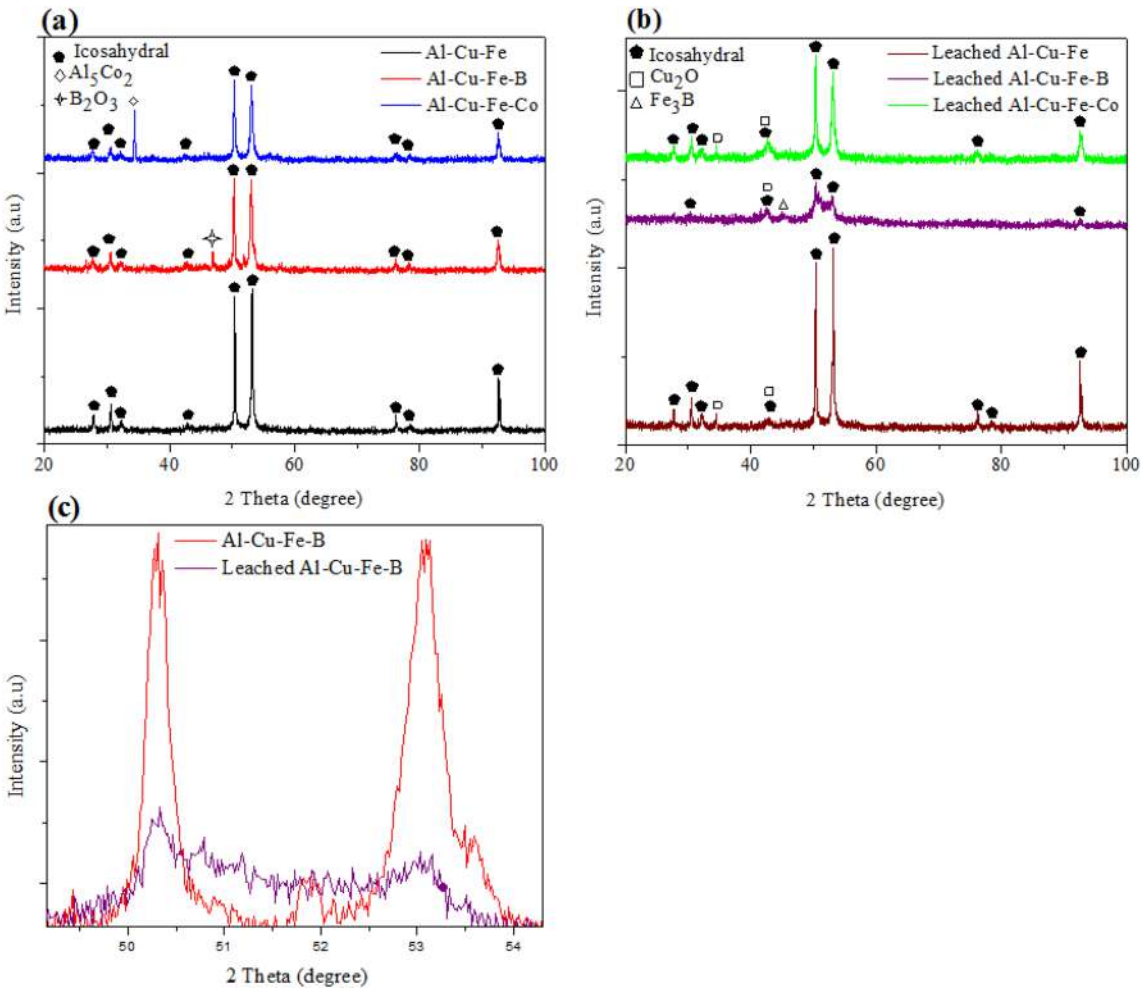

Fig. 1 Powder X-ray diffraction patterns of Al–Cu–Fe, Al–Cu–Fe–B and Al–Cu–Fe–Co powder samples before leaching (**a**), after leaching (**b**) and peak broadening in Al–Cu–Fe–B due to the leaching process (**c**)

alloyed in a RETSCH PM-200 planetary ball mill to prepare $Al_{65}Cu_{23}Fe_{11}B$ and $Al_{65}Cu_{23}Fe_{11}Co$ QC powders. Hardened steel vial and balls (diameter 10 mm) were used as the milling media, while n-hexane was used as a process control agent. The ball-to-powder weight ratio was set to 10:1, and milling was performed at 250 rpm for 50 h. Subsequently, the milled powder was cold pressed in a uniaxial cold press under the load of 208 MPa and the dwell time of 15 min. Finally, the green powder samples were separately vacuum hot pressed for 5 h (at temperature and pressure of 700 °C and 130 MPa, respectively) to achieve icosahedral phase. Subsequently, the pressed Al–Cu–Fe, Al–Cu–Fe–B and Al–Cu–Fe–Co QCs were ground by pestle and mortar to obtain fine powder. The fine powders were then leached for 2 h in 10 M NaOH aqueous solution maintained at 50 °C under continuous stirring. Finally, the leached powders were filtered out and washed two to three times with distilled water and ethanol. The washed QC powders were dried overnight in an oven maintained at 75 °C.

2.2 Characterization

The Al–Cu–Fe, Al–Cu–Fe–B and Al–Cu–Fe–Co QC powders were characterized by scanning electron microscopy (SEM), energy-dispersive X-ray (EDX) spectrometer, pycnometer and differential scanning calorimetry (DSC). The crystal structure of QCs was determined by X-ray diffraction (XRD) (Philips PW 1050 Bragg–Brentano diffractometer) using Co-*K*α radiation ($\lambda = 0.17889$ nm). The compositional analysis of the leached solution of Al–Cu–Fe QCs was carried out by inductive coupled plasma optical emission spectroscopy (ICP-OES). Morphological analysis of the QCs was carried out using NOVA-NANOSEM 430 field emission scanning electron microscope. The density of the prepared QCs was measured before and after leaching by AccuPyc-II 1340 Pycnometer. The thermal stability of Al–Cu–Fe and Al–Cu–Fe–Co QCs was determined by SDT Q600 differential scanning calorimeter (DSC).

2.3 Agar diffusion test for antimicrobial activity

Antimicrobial properties of synthesized samples were determined by agar diffusion test using Gram-negative (*E. aerogenes, K. pneumoniae)* and Gram-positive (*B. cereus, K. rosea)* bacteria [23]. The bacteria were cultured in Luria–Bertani (LB) broth, prepared by dissolving 1% (w/v) tryptone, 0.5% (w/v) NaCl and 0.5% (w/v) of yeast extract in distilled water followed by sterilization in autoclave at 120 °C and 15 psi pressure for 15 min. Bacteria were grown overnight at 37 °C in 100 ml conical flask (containing 10 ml of LB broth) placed in shaking incubator (I-4000 IRMECO GmbH, Germany) rotating at the speed of 100 rpm. The LB agar was prepared by dissolving 1.5% (w/v) agar in LB broth followed by sterilization for 15 min in the autoclave (Tomy Seiko Co. Ltd., Japan, SX-500) at temperature and pressure of 120 °C and 15 psi, respectively. The solidified LB agar was first melted in a microwave oven, and then, 20 ml of liquefied LB agar was poured into sterilized petri dishes which were allowed to solidify under sterilized conditions. A lawn of bacterial culture was prepared by spreading 200 µl of each of culture test bacteria over the dry surface of agar plates using sterilized glass spreader. The bacteria were allowed to be absorbed on the surface. The suspensions of leached and un-leached Al–Cu–Fe, Al–Cu–Fe–B and Al–Cu–Fe–Co QC powders and copper powder with the concentration of 1 mg/µl were prepared in distilled water. The 5 µl spot of QC powder suspensions, copper powder suspension, kanamycin (concentration 0.5×10^{-1} mg/µl) and ampicillin (concentration 100 mg/ml) were spotted on the surface of seeded agar plates. Kanamycin and ampicillin are used as a positive control, and copper is used for comparison. After incubation at 37 °C overnight, the diameters of zones of inhibition were measured. The experiment on *E. aerogenes* was repeated for five times.

3 Results and discussion

Before investigating antimicrobial properties, the synthesized powder samples were characterized by different techniques in order to examine their structure, surface morphology and chemical composition. The powder X-ray diffraction (XRD) patterns of the spray-deposited (Al–Cu–Fe)

Table 1 Average grain size calculated by Scherrer's formula

Sample	Average grain size (nm)	
	Before leaching	After leaching
Al–Cu–Fe	> 1000 [31]	120.57
Al–Cu–Fe–B	122.38	73.31
Al–Cu–Fe–Co	122.49	104.74
Cu_2O of Al–Cu–Fe	–	19.96
Cu_2O of Al–Cu–Fe–B	–	31.82
Cu_2O of Al–Cu–Fe–Co	–	19.90
B_2O_3	86.04	–
Fe_3B	–	20.84
Al_5Co_2	141.63	–

Table 2 ICP-OES analysis of leached solution of spray-deposited Al–Cu–Fe

Element	Dissolution (ppm)
Al	2803
Cu	76
Fe	46

and hot-pressed (Al–Cu–Fe–B, Al–Cu–Fe–Co) powder samples, before and after leaching treatment in 10 M NaOH aqueous solution, are shown in Fig. 1. The XRD pattern in Fig. 1a shows that the un-leached precursor powder samples mostly contain single-phase icosahedral quasicrystals [24]. Moreover, minor quantities of B_2O_3 and Al_5Co_2 phases are also present in Al–Cu–Fe–B and Al–Cu–Fe–Co samples, respectively. The XRD scans reveal that after leaching treatment, the icosahedral structure remains intact in all the three powder samples. The peak, related to Al_5Co_2 phase, vanishes after leaching treatment which indicates the dissolution of the aluminum-rich intermetallic phase in NaOH solution. Moreover, small peaks at 34° and 43° indicate formation of Cu_2O cubic phase in all the three samples, as shown in Fig. 1b. Another peak is found at 45.35° which can be associated with the formation of Fe_3B in Al–Cu–Fe–B

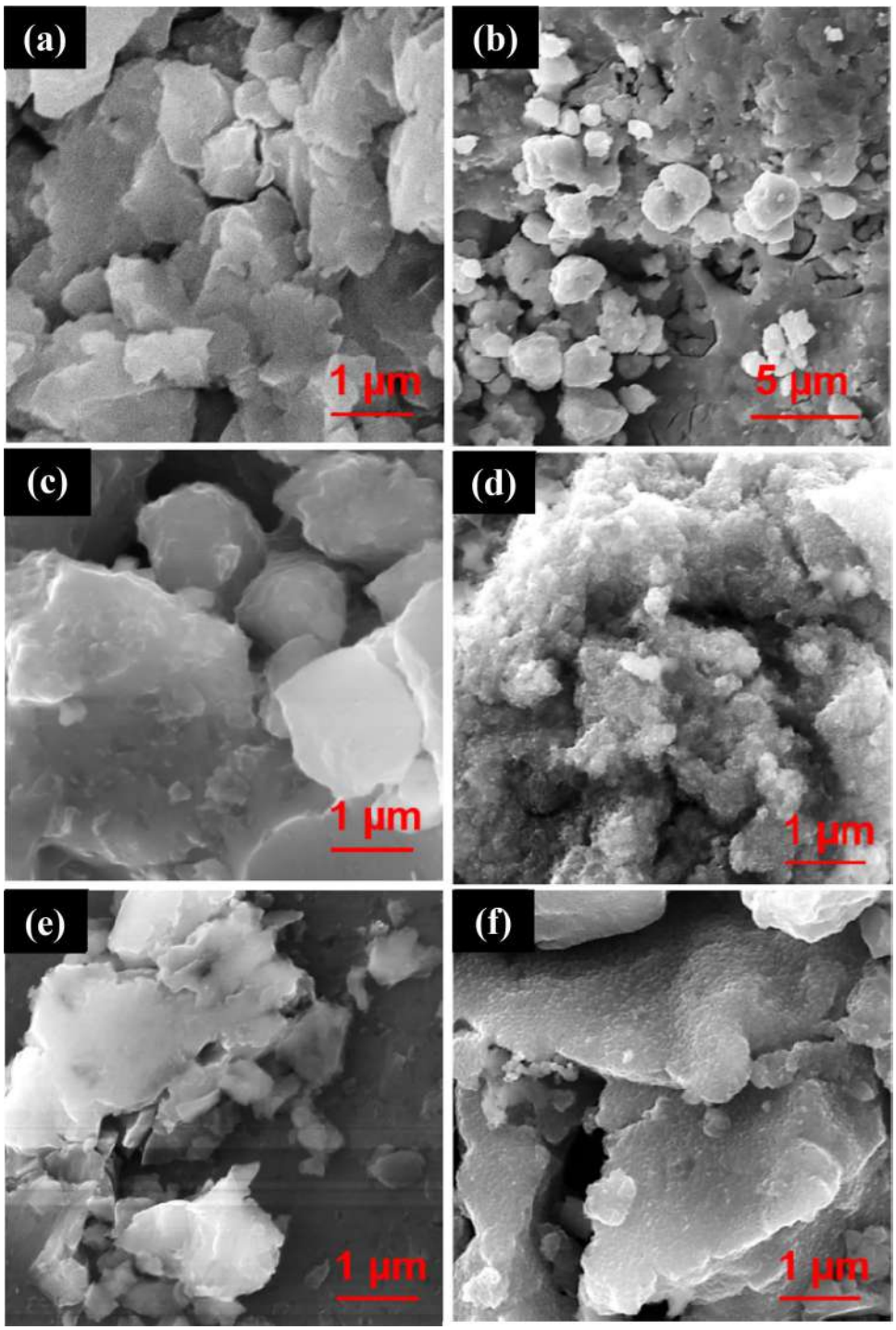

Fig. 2 SEM images of Al–Cu–Fe (**a**), leached Al–Cu–Fe (**b**), Al–Cu–Fe–B (**c**), leached Al–Cu–Fe–B (**d**), Al–Cu–Fe–Co (**e**) and leached Al–Cu–Fe–Co (**f**) powder samples

alloy sample. It is interesting to note that the XRD peaks of Al–Cu–Fe–B alloy are significantly broadened due to the leaching process (Fig. 1c). This peak broadening seems to be attributed to the reduction in quasi-crystallite size in the leached Al–Cu–Fe–B alloy. Sordelet et al. also reported similar peak broadening phenomena for $Al_{62}Cu_{25}Fe_{12}B$ alloy [25]. The leaching process causes selective dissolution of aluminum from the surface. Consequently, Cu- and Fe-rich structures are formed at the surface [26]. Dissolution of Al in Al–Cu–Fe–B sample is distinctly pronounced as compared to those of other samples (discussed later in this section). This leads to significant compositional changes at the surface which might create structural defects and result in the peak broadening [26]. The average grain size of all the prepared powder samples was calculated using Scherrer's formula, and the results are summarized in Table 1. After leaching treatment, average grain size of icosahedral quasicrystal is remarkably reduced. Table 1 also indicates formation of a nano-crystalline Cu_2O phase in the leached samples [20]. Difference in composition as well as processing route of quasicrystals affected their grain size. The Al–Cu–Fe–B and Al–Cu–Fe–Co quasicrystal powders, prepared through mechanical alloying and subsequent hot pressing, show smaller grain size when compared with that of thermally sprayed Al–Cu–Fe powder.

The ICP analysis of the leached Al–Cu–Fe spray-deposited powder indicates the removal of significant amount of Al along with the dissolution of very small amount of Cu and Fe (Table 2). It can be deduced from the results that unlike Al atoms, the most of Cu and Fe atoms remain intact on the surface.

The scanning electron microscopy (SEM) images formed by using secondary electrons, of the all powder samples, before and after leaching treatment, are shown in Fig. 2. Before leaching (Fig. 2a, c, and e), the surface of the powder samples appears relatively smooth in comparison with the leached surface. During leaching, significant dissolution of Al in alkaline solution results in uneven surface morphology (Fig. 2b, d, and f). It is shown clearly in Fig. 2b that the leaching process has dissolved few regions of the surface thereby creating a polygonal type of pores. This pore morphology can be formed during leaching due to preferential dissolution in a particular direction [14]. Longer leaching time resulted in intense dissolution, expansion in pore size and weakening/cracking of the local surface. This eventually leads partial spalling off the surface in the form of fine particles as highlighted in Fig. 2b [14]. The grain size of mechanically milled/hot-pressed Al–Cu–Fe–B, Al–Cu–Fe–Co powder samples is much finer than that of the spray-deposited Al–Cu–Fe sample. After leaching, these nanostructured samples containing boron and cobalt produced much smaller-scale surface features. This can be attributed to the enhancement of surface activity due to the

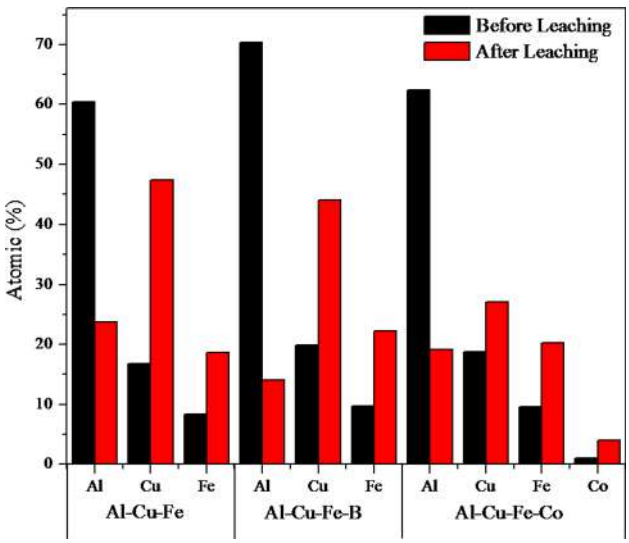

Fig. 4 Energy-dispersive X-ray (EDX) analysis of Al–Cu–Fe, Al–Cu–Fe–B and Al–Cu–Fe–Co powder samples before and after leaching

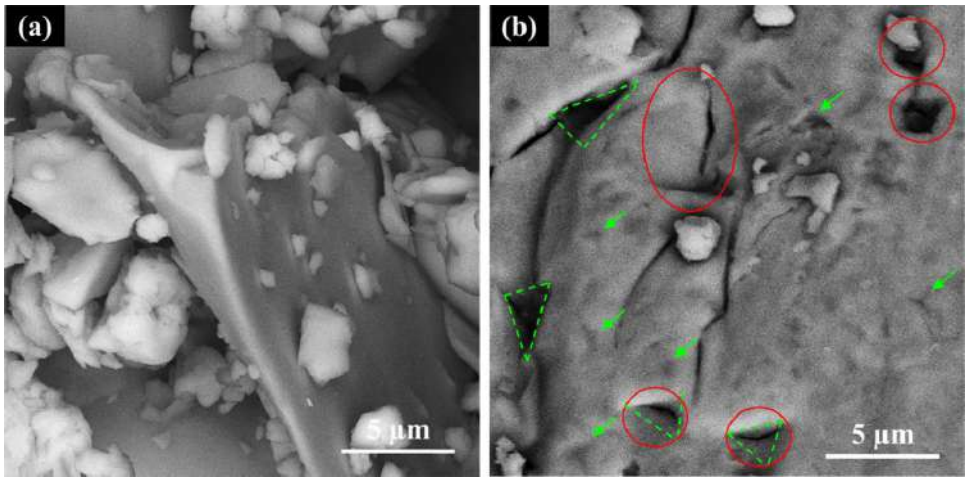

Fig. 3 BSE images of Al–Cu–Fe powder sample before (**a**) and after leaching (**b**)

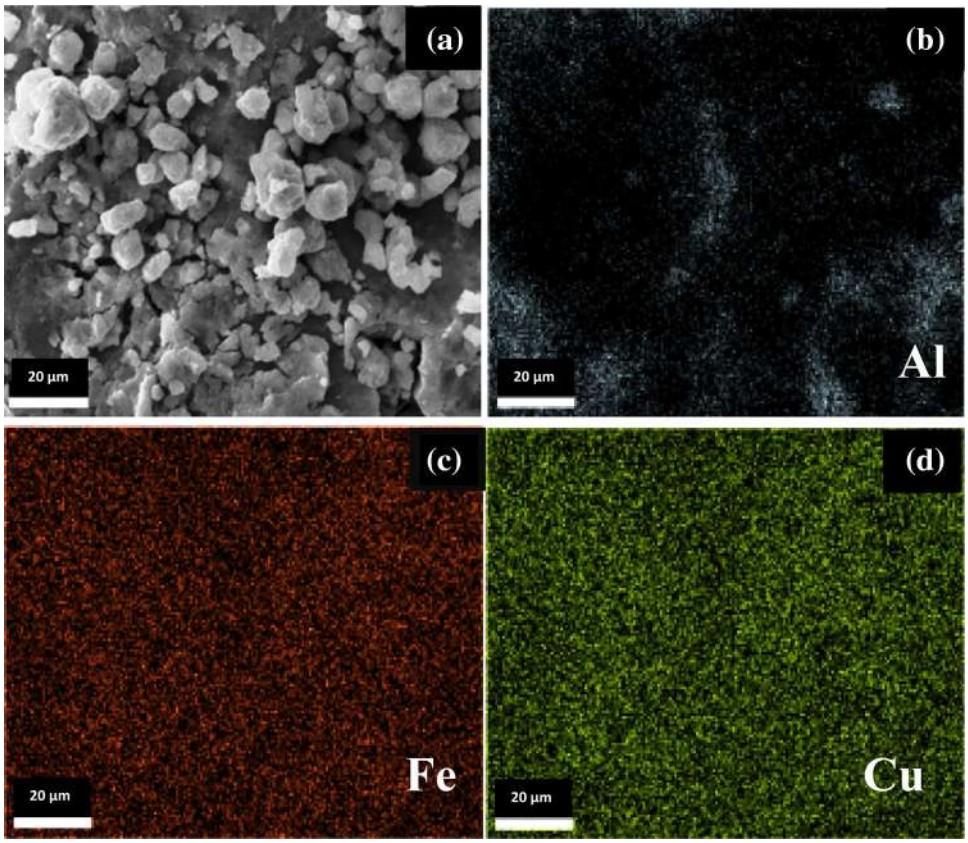

Fig. 5 Energy-dispersive X-ray (EDX) mapping of leached Al–Cu–Fe powder

grain refinement [27]. Boron-containing leached surface consists of fine granular particles with few flake-like particles (of size ~ 300 nm) distributed among them (Fig. 2d). On the other hand, the leached Al–Cu–Fe–Co has granulated surface with ~ 100 nm asperities (Fig. 2f). Change in the morphology of surface, during leaching process, can either be due to a change in surface dissolution kinetics (which may be promoted due to the presence of B or Co atoms in the surface) or the presence of higher number of grain boundaries in both samples.

The backscattered SEM images of the spray-deposited Al–Cu–Fe powder sample, before and after leaching, are shown in Fig. 3. Before leaching, surface shows a uniform appearance, while multiple dark spots are observed on the leached surface. The presence of triangular dark spots in SEM image is due to Z-number contrast, and it indicates non-uniform composition at the surface. Cu and Fe appear

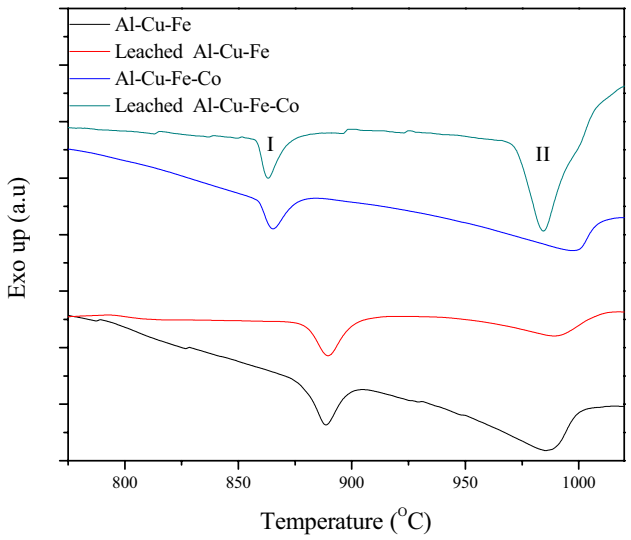

Fig. 6 DSC curves before and after leaching of Al–Cu–Fe and Al–Cu–Fe–Co powder samples

Table 3 Enthalpies of structural transformations of powder samples obtained through DSC

Sample	Temperature (°C)	Enthalpy (ΔH) kJ/mol
Al–Cu–Fe	890	114.4
	985	214.5
Leached Al–Cu–Fe	890	100.1
	990	157.3
Al–Cu–Fe–Co	865	14.3
	998	200.2
Leached Al–Cu–Fe–Co	863	71.5
	985	343.2

brighter than Al. The *Z*-contrast between Cu and Fe is very small, so it is difficult to differentiate between them. Cavities and triangular spots (with darker contrast) indicate Al-rich regions as shown in Fig. 3b. Since the leaching solution preferably attacks Al atoms from the surface, Al-rich regions can be considered as the preferred sites for surface dissolution during leaching. This leads to formation of pores at Al-rich sites as shown in Fig. 3b. It can be inferred that Al-rich sites or Al-rich phases may enhance pore formation at the surface.

Energy-dispersive X-ray (EDX) analysis of Al–Cu–Fe, Al–Cu–Fe–B and Al–Cu–Fe–Co powder samples is shown in Fig. 4. It shows that most of the Al dissolves from the surface after leaching treatment, leaving behind the dense surface rich in Cu and Fe [28]. It also indicates that boron-containing icosahedral surface readily and more preferentially dissolves aluminum in comparison with copper (with Cu atoms/Al atoms ratio increasing to ~ 3 at the leached surface). EDX mapping of the leached Al–Cu–Fe alloy powder is shown in Fig. 5. Color mapping confirms that the surface is richer in Cu and Fe. The helium-based pycnometer density of the powders (before and after leaching) increases from 4.4 to 4.6 g/cm^3. This increase in the density after leaching is attributed to the formation of dense surface containing Cu and Fe. Due to immiscibility of Fe and Cu atoms in solid solution, the presence of Fe atoms at the surface hinders atomic diffusion of Cu thereby inhibiting Cu agglomeration [14]. As a result, stabilized surface structure with dispersed nano-sites of Cu/Cu_2O is formed [18]. The literature shows that the presence of dispersed Cu sites on metallic components could enhance their antimicrobial behavior [29].

Thermal stability of the contact killing surface is very important for their use under different conditions. Therefore, differential scanning calorimetry (DSC) was used to determine the thermal stability of the icosahedral phase. The DSC curves of Al–Cu–Fe and Al–Cu–Fe–Co (before and after leaching treatment) are shown in Fig. 6. No distinct peak is observed below 850 °C. Two endothermic peaks can be observed in all curves. The first endothermic peak (at temperature ≥ 863 °C) could be associated with transformation of icosahedral phase to cubic Al(Cu,Fe) (β-phase), Al_3Fe (λ-phase) and liquid phase. The second endothermic peak (at temperature ≥ 985 °C) is related with the formation

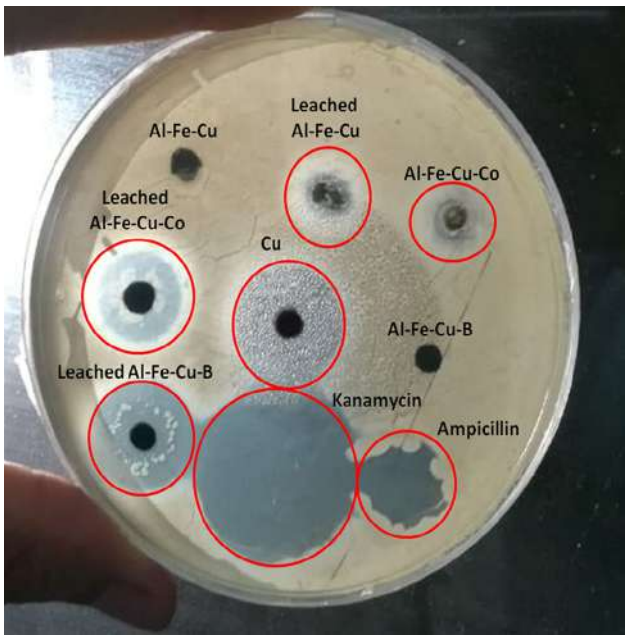

Fig. 8 Agar petri dish showing DIZ of different samples against *E. aerogenes*

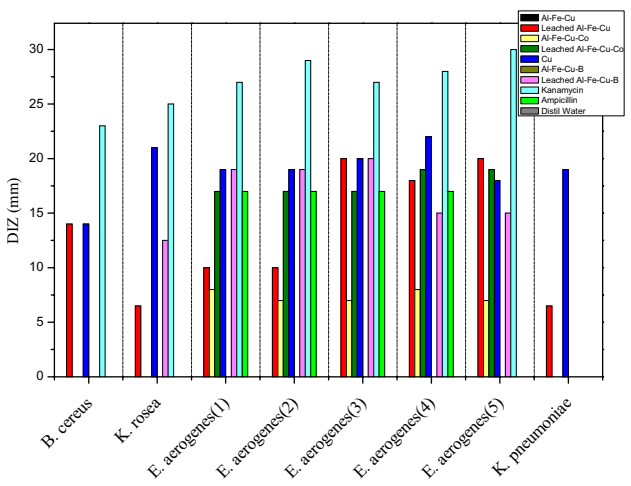

Fig. 7 Diameter of inhibition zone (DIZ) in agar diffusion test exhibited by different samples against tested bacteria

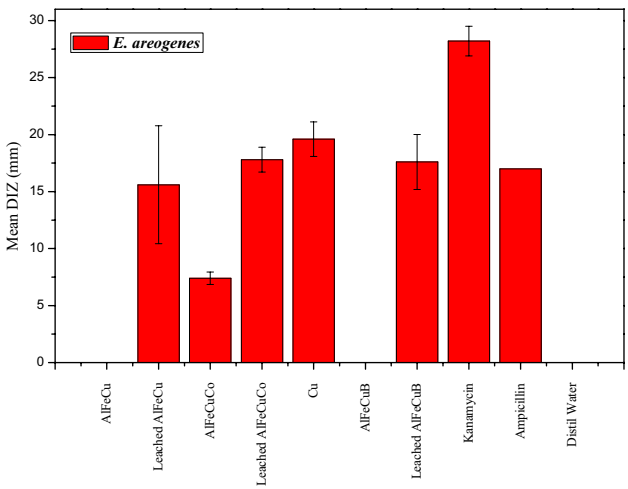

Fig. 9 Average diameter of inhibition zone (DIZ) exhibited by different samples against *E. aerogenes*

Table 4 Mean DIZ of *E. aerogenes* for different samples

Powder samples	Conc. (mg/ul)	Amount of suspension solution (µl)	DIZ of *E. aerogenes* (mm)	References
Al–Fe–Cu	1	5	0	Present work
Leached Al–Fe–Cu	1	5	15.6 ± 5.2	
Al–Fe–Cu–Co	1	5	7.4 ± 0.5	
Leached Al–Fe–Cu–Co	1	5	17.8 ± 1.1	
Cu	1	5	19.6 ± 1.5	
Al–Fe–Cu–B	1	5	0	
Leached Al–Fe–Cu–B	1	5	17.6 ± 2.4	
Kanamycin	0.5×10^{-4}	5	28.2 ± 1.3	
Ampicillin	1×10^{-4}	5	17	
Distilled water	–	5	0	
CuO (nanoparticle)	–	20	14	[36]
$Hg[Cu(C_{17}H_{16}N_2O_2)SCN]_2$	–	20	12	[37]
$Hg[Cu(C_{18}H_{18}N_2O_2)SCN]_2$	–	20	12	
$C_{24}H_{31.39}CuN_2O_{4.70}$	10^{-3}	90	15.33 ± 0.47	[38]

of complete liquid phase [30]. The change in enthalpy (ΔH), at different temperatures, is summarized in Table 3. Clearly, the value of ΔH decreases with leaching due to decrease in Al/(Cu, Fe) ratio which is important for the stability of icosahedral phase [31].

To study antimicrobial properties of the prepared powder samples, agar diffusion test was conducted at 37 °C. All tests were carried out on Gram-negative (*E. aerogenes, K. pneumoniae*) and Gram-positive (*B. cereus, K. rosea*) bacteria. The diameters of inhibition zone (DIZ) obtained against these bacteria are shown in Fig. 7. It is interesting to note that the leached powder samples show greater DIZ as compared to the un-leached powders. The powder suspensions (with the concentration of 1 mg/µl) were prepared in distilled water. In order to ensure that distilled water has no influence on the DIZ, 5 µl of it was added to agar plate. The distilled water did not show any DIZ which clearly indicates that antimicrobial properties are entirely due to the powder samples.

Interestingly, the DIZ of the leached quasicrystalline surfaces is comparable to that of copper and ampicillin, while it is less than that of kanamycin. Antimicrobial properties can be enhanced by increasing specific surface area [32–34] or by increasing the number of active sites [35]. The ability of leached quasicrystalline surface, to produce increased DIZ, may be attributed to the formation of uniformly dispersed nano-sized Cu/Cu_2O sites (with high specific surface area) on the surface of icosahedral quasicrystals. Although, Fe does not play a direct role in producing DIZ, but its presence in the leached surface stabilizes Cu/Cu_2O nano-sites which is important in enhancing antimicrobial surface characteristics [14]. Remarkable antimicrobial properties of the leached icosahedral surface could also be associated with the higher activity of copper atoms on the icosahedral surface due to its smaller coordination number as compared to FCC structure [33].

The DIZ shows the lethality of samples on the bacteria [32]. DIZs of samples against *E. aerogenes* are shown in Fig. 8. DIZ of *E. aerogenes* is comparatively higher than that of other bacteria; hence, it is most susceptible to the leached powder samples. In order to ensure accuracy, experiments were repeated five times on *E. aerogenes* and the average DIZs were calculated as shown in Fig. 9. Table 4 clearly shows that the mean DIZ of leached quasicrystals against *E. aerogenes* is superior to other Cu-based alloys/compound reported in the studies [36–38].

Inherent hardness (1000 Hv) and low friction coefficient [17] of Al–Cu–Fe quasicrystals together with their contact killing ability for bacteria make them a potential candidate for coating material for commonly touched surfaces like bed rails, door handles, etc., in the hospitals or other similar places where both wear resistance and anti-bacterial characteristics are required.

4 Conclusion

In this novel study, we demonstrated the antimicrobial properties of the spray-deposited Al–Cu–Fe and hot-pressed Al–Cu–Fe–B and Al–Cu–Fe–Co QCs. Leaching in alkaline aqueous solution of NaOH did not change icosahedral structure of QCs which is confirmed by XRD. BSE and EDX show that leached surface becomes poor in Al and enriched in Cu and Fe. Leached QCs show prominent antimicrobial properties. Our results indicate that *E. aerogenes*is are most susceptible to leached QC surfaces among the bacteria

tested. Leached Al–Cu–Fe–Co and Al–Cu–Fe–B QCs show greater DIZ in comparison with Al–Cu–Fe QCs. Therefore, leached QCs can be promising materials to reduce the microbial burden from commonly touched surfaces such as bed rails, faucets and doorknobs in hospitals to reduce the number of hospital-acquired infections.

Acknowledgement Authors would like to acknowledge support provided by PIEAS.

References

1. N. Cioffi, N. Ditaranto, L. Torsi, R.A. Picca, E. De Giglio, L. Sabbatini, L. Novello, G. Tantillo, T. Bleve-Zacheo, P. Zambonin, Anal. Bioanal. Chem. **382**, 1912–1918 (2005)
2. The direct medical costs of healthcare-associated infections in U.S. hospitals and the benefits of prevention (2009). Retrieved May 16, 2020 from https://www.cdc.gov/HAI/pdfs/hai/Scott_CostPaper.pdf
3. H. Parsamehr, Y.J. Lu, T.Y. Lin, A.P. Tsai, C.H. Lai, Sci. Rep. **9**, 1–9 (2019)
4. D. Shechtman, I. Blech, D. Gratias, J.W. Cahn, Phys. Rev. Lett. **53**, 1951 (1984)
5. I. Hargittai, Isr. J. Chem. **51**, 1144–1152 (2011)
6. L. Bendersky, Phys. Rev. Lett. **55**, 1461 (1985)
7. H. Chen, D. Li, K. Kuo, Phys. Rev. Lett. **60**, 1645 (1988)
8. A. Pope, T.M. Tritt, *Thermal Conductivity of Quasicrystalline Materials, Thermal Conductivity* (Springer, New York, 2004), pp. 255–259
9. Y. Honda, K. Edagawa, A. Yoshioka, T. Hashimoto, S. Takeuchi, Jpn. J. Appl. Phys. **33**, 4929 (1994)
10. S. Takeuchi, H. Iwanaga, T. Shibuya, Jpn. J. Appl. Phys. **30**, 561 (1991)
11. J.-M. Dubois, Chem. Soc. Rev. **41**, 6760–6777 (2012)
12. J.-M. Dubois, E. Belin-Ferré, Appl. Adhesion Sci. **3**, 28 (2015)
13. E. Huttunen-Saarivirta, T. Tiainen, Mater. Chem. Phys. **85**, 383–395 (2004)
14. M. Lowe, T. Yadav, V. Fournée, J. Ledieu, R. McGrath, H. Sharma, J. Chem. Phys. **142**, 094703 (2015)
15. R.M. Klevens, J.R. Edwards, C.L. Richards Jr., T.C. Horan, R.P. Gaynes, D.A. Pollock, D.M. Cardo, Public Health Rep. **122**, 160–166 (2007)
16. P.D. Bloom, K. Baikerikar, J.U. Otaigbe, V.V. Sheares, Mater. Sci. Eng. A **294**, 156–159 (2000)
17. M. Besser, T. Eisenhammer, MRS Bull. **22**, 59–63 (1997)
18. A. Tsai, M. Yoshimura, Appl. Catal. A **214**, 237–241 (2001)
19. S. Kameoka, T. Tanabe, A.P. Tsai, Catal. Today **93**, 23–26 (2004)
20. T. Tanabe, S. Kameoka, A.P. Tsai, Appl. Catal. A **384**, 241–251 (2010)
21. Copper kills bacteria: end of hospital-acquired infections? (n.d.). Retrieved May 16, 2020 from http://www.scienceonthenet.eu/content/article/marc-solioz/copper-kills-bacteria-end-hospital-acquired-infections/april-2011
22. V.C. Srivastava, V. Uhlenwinkel, A. Schulz, H.W. Zoch, N.K. Mukhopadhyay, S.G. Chowdhury, Zeitschrift für Kristallographie. Int. J. Struct. Phys. Chem. Aspects Cryst. Mater. **223**, 711–715 (2008)
23. J.M. Andrews, f.t. BSAC working party on susceptibility testing. J. Antimicrobial. Chemother. **48**, 43–57 (2001)
24. N. Mukhopadhyay, F. Ali, V. Srivastava, T. Yadav, M. Sakaliyska, K. Surreddi, S. Scudino, V. Uhlenwinkel, J. Eckert, Philos. Mag. **91**, 2482–2490 (2011)
25. D. Sordelet, T. Bloomer, M. Kramer, O. Unal, J. Mater. Sci. Lett. **15**, 935–939 (1996)
26. I. Yamauchi, M. Ohmori, I. Ohnaka, J. Alloys Compd. **299**, 269–275 (2000)
27. S. Kameoka, T. Tanabe, F. Satoh, M. Terauchi, A.P. Tsai, Sci. Technol. Adv. Mater. **15**, 014801 (2014)
28. T. Yadav, S. Mishra, S. Pandey, D. Singh, M. Lowe, R. Tamura, N. Mukhopadhyay, O. Srivastava, R. McGrath, H. Sharma, Acta Phys. Pol. A **126**, 629 (2014)
29. M.S. Usman, M.E. El Zowalaty, K. Shameli, N. Zainuddin, M. Salama, N.A. Ibrahim, Int. J. Nanomed. **8**, 4467 (2013)
30. V. Srivastava, E. Huttunen-Saarivirta, C. Cui, V. Uhlenwinkel, A. Schulz, N. Mukhopadhyay, J. Alloys Compd. **597**, 258–268 (2014)
31. F. Ali. Mechanical milling of Al-Cu-Fe quasicrystals and their reinforcement in aluminum matrix composites. Verlag nicht ermittelbar (2012)
32. Z. Yang, X. Hao, S. Chen, Z. Ma, W. Wang, C. Wang, L. Yue, H. Sun, Q. Shao, V. Murugadoss, J. Colloid Interface Sci. **533**, 13–23 (2019)
33. A. Azam, A.S. Ahmed, M. Oves, M. Khan, A. Memic, Int. J. Nanomed. **7**, 3527 (2012)
34. M. Vincent, R.E. Duval, P. Hartemann, M. Engels-Deutsch, J. Appl. Microbiol. **124**, 1032–1046 (2018)
35. A. Harada, H. Ichimaru, T. Kawagoe, M. Tsushida, Y. Niidome, H. Tsutsuki, T. Sawa, T. Niidome, Bull. Chem. Soc. Japan **92**, 297–301 (2019)
36. Y. Abboud, T. Saffaj, A. Chagraoui, A. El Bouari, K. Brouzi, O. Tanane, B. Ihssane, Appl. Nanosci. **4**, 571–576 (2014)
37. L.T. Yıldırım, R. Kurtaran, H. Namli, A.D. Azaz, O. Atakol, Polyhedron **26**, 4187–4194 (2007)
38. S.S. Batool, S.R. Gilani, S.S. Zainab, M.N. Tahir, W.T. Harrison, M.S. Haider, Q. Syed, S. Mazhar, M. Shoaib, Polyhedron **178**, 114346 (2020)